J Therm Spray Tech (2023) 32:1350–1361
https://doi.org/10.1007/s11666-023-01568-4

PEER REVIEWED

Effects of SiC on Microstructure and Properties of Coatings Prepared by Plasma Spraying Cr_2O_3-Al-SiC Powder

Pei-wen Ru[1] · Yong Yang[1] · Yu-ping Zhao[1] · Wei Tian[2] · Yu-xuan Shao[1] · Yan-wei Wang[1] · Wei Li[1] · Yu-duo Ma[1]

Submitted: 27 August 2022 / in revised form: 14 January 2023 / Accepted: 19 January 2023 / Published online: 16 March 2023

Abstract Four kinds of chromium carbide composite coatings were successfully prepared on the surface of TC4 titanium alloy by plasma spraying Cr_2O_3-Al-SiC composite powder. The effects of SiC content in composite powder on the microstructure and properties of the as-prepared coatings were investigated. The results showed that the desired phases of Cr_7C_3, $CrSi_2$ and Al_2O_3 were synthesized in situ through the reactions among Cr_2O_3, Al and SiC powders. However, due to the different content of each phase in coatings, the microstructure and properties were different. When the SiC content increased from 5 to 12 wt.%, the porosity of the coatings decreased, and the microhardness and toughness increased. Continue to increase SiC content to 19 and 30 wt.%, the porosity of the coatings increased, and the microhardness and toughness decreased. When the SiC content was 12 wt.%, the as-prepared coating had the lowest porosity (3.20%), the highest microhardness (1262.2 $HV_{0.1}$) and the best fracture toughness (3.3 MPa $m^{1/2}$) due to the higher reaction degree and better melting state of the composite powders in the plasma jet.

Keywords Cr_2O_3-Al-SiC · microstructure · plasma spraying · properties · SiC content

✉ Yong Yang
yangyonghebut@163.com; yangyong@hebut.edu.cn

[1] Key Lab. for New Type of Functional Materials in Hebei Province, School of Materials Science and Engineering, State Key Laboratory of Reliability and Intelligence of Electrical Equipment, Tianjin Key Laboratory of Materials Laminating Fabrication and Interface Control Technology, Hebei University of Technology, Tianjin 300132, People's Republic of China

[2] AECC Sichuan Gas Turbine Establishment, Sichuan Province, Chengdu 610500, People's Republic of China

Introduction

Transition metal carbide chromium carbide (Cr_7C_3) has high melting point, high hardness, good corrosion resistance and excellent high-temperature stability. Using Cr_7C_3 as coating material has obvious advantages. Due to its excellent physical and chemical properties, it can be applied to the surface of metal or alloy through various surface technologies, so as to improve the service life of wear-prone components (Ref 1-3). Cr_7C_3 coating has broad application prospects in the field of material protection (Ref 4). Because of the high melting point of Cr_7C_3, it is prone to oxidation and decarburization in high-temperature environment. Moreover, Cr_7C_3 has the inherent brittleness of ceramic materials, so single-phase Cr_7C_3 powder is rarely used as coating material alone, but mostly used as reinforcing phase or combined with other alloy phases or ceramics to improve coating performance. Liu et al. (Ref 5) used plasma jet cladding technology to prepare a coating on a Q235 carbon steel substrate using Ni-Cr-C elemental powder blends. The coating was composed of primary coarse blocky carbide Cr_7C_3 and the inter-blocky tough γ-Ni/Cr_7C_3 eutectic matrix. The composite coating had high hardness and excellent wear resistance in dry sliding wear test. Niu et al. (Ref 6) prepared Ni_3Si-Cr_7C_3 composite coating on AISI 1020 steel substrate by self-propagating high-temperature synthesis (SHS) casting route and explored the effect of phase composition in the coating on the microhardness and dry sliding wear behavior of the coating. The results showed that the high hardness of the composite coating was due to the existence of Cr_7C_3 phase. The microhardness of the coating increases significantly with the increase of Cr_7C_3 volume fraction. Zhu et al. (Ref 7) prepared Cr_7C_3-$(Ni, Cr)_3(Al, Cr)$ coating by HVOF. The major phases of the as-prepared coating were Cr_7C_3 and Cr

alloyed Ni_3Al. With the increase of Cr_7C_3 content, the room temperature microhardness of the composite coating increased. When the Cr_7C_3 content was too high, the room temperature hardness will decrease because the hard ceramic phase lacks the support of the binder phase.

In order to reduce the brittleness of chromium carbide, an important way is to prepare multiphase ceramic coating. Compared with single-phase ceramics, multiphase ceramics not only have better hardness, but also have better fracture toughness. The fracture toughness of ternary composites is higher than that of binary composites (Ref 8, 9). Composite coating combines the advantages of each phase, and its performance is significantly better than that of single-component ceramic coating (Ref 10). Transition metal silicides are widely used as high-temperature structural materials due to their good high-temperature oxidation resistance, high-temperature creep strength and high-temperature acid corrosion resistance (Ref 11). Chromium silicide ($CrSi_2$) is an important silicide. First, its melting point (1490 °C) is relatively low, which can fill the pores and cracks of the as-prepared coating and reduce the porosity of the as-prepared coating (Ref 12); second, the SiO_2 glass formed in high-temperature oxidation atmosphere has good oxidation resistance (Ref 13); third, the thermal expansion coefficient (TEC) of $CrSi_2$ (10.5×10^{-6} k^{-1}) and Cr_7C_3 (10.0×10^{-6} k^{-1}) is similar, which can reduce the thermal stress in the coating during the cooling process of thermal spraying and reduce the generation of cracks. By introducing low melting point component chromium silicide into the coating, not only the brittleness of chromium carbide can be reduced, but also the overall thermal shock resistance and high-temperature oxidation resistance of the coating can be improved. Ma et al. (Ref 14) used Cr-SiC composite powder as raw material to prepare Cr_7C_3-$CrSi_2$ composite coating by plasma spraying technology. The results showed that Cr and SiC in Cr-SiC composite powder had obvious chemical reaction. The as-prepared coating included chromium carbide (Cr_7C_3 and Cr_3C_2) and chromium silicide ($CrSi_2$). The coating structure was uniform and dense, with high hardness (1003.3 $HV_{0.1}$), low wear rate and good toughness.

Atmospheric plasma spraying (APS) technology is a suitable choice for preparing high-quality ceramic coatings because of its low cost, flexible process and wide variety of sprayable materials (Ref 15, 16). Atmospheric plasma spraying combined with self-propagating high-temperature synthesis technology is reactive plasma spraying (RPS) technology. RPS is based on the reactions between the sprayed materials and surrounding reactive gases in the plasma or mutual reactions with constituents in feedstock powders. In recent years, RPS has been widely used to prepare ceramic matrix composite coatings (Ref 17–22). RPS has great advantages. It can form fine and uniformly dispersed stable hard phase in situ, and can prepare multi-performance and high-quality composite coatings with cheap raw materials (Ref 23, 24). Since the powders of the target component are not sprayed directly, the component of the precursor powder has a great impact on the type of the synthesized target product and the quality of the prepared coating. Xu et al. (Ref 25) prepared TiB_2-TiC-Al_2O_3/Al composite coatings on the surface of magnesium alloy substrate by reactive plasma spraying Al-TiO_2-B_4C system. The results showed that with the increase of Al content, the coatings became much denser, but the microhardness of the coatings gradually decreased. The composition of precursor powder has a great influence on the microstructure and properties of the coating.

In the present investigation, the precursor composite powder of Cr_2O_3-Al-SiC aluminothermic reaction system was used to prepare chromium carbide composite coating by atmospheric plasma spraying technology. In this system, the high exothermic property of the thermite reaction between Cr_2O_3 and Al is conducive to the full melting of powder particles, and the by-product Al_2O_3 can also improve the hardness and wear resistance of the coating (Ref 26). By changing the SiC content in Cr_2O_3-Al-SiC composite powder, four different coatings were prepared under the same process parameters. The effects of SiC content on the microstructure and properties of the as-prepared coatings were investigated. This study can provide some reference experience for the development of reactive plasma spraying and the preparation of chromium carbide composite coating.

Experimental Materials and Characterization Methods

In this study, commercial available Cr_2O_3 powder (Hebei Xingtai Huana Metal Materials Co., Ltd.), Al powder (Angang Industrial Fine Aluminum Powder Co., Ltd.) and SiC powder (Shandong Weifang Kaihua Silicon Carbide Powder Co., Ltd.) were selected as raw materials. The particle size of Cr_2O_3 raw powders was between 1 and 2 μm, the particle size of Al raw powders was between 6 and 9 μm and the particle size of SiC raw powders was between 1 and 3 μm. Equation (1) was the aluminothermic reaction equation of Cr_2O_3 and Al at precise stoichiometric ratio. Here, on the premise of ensuring that the molar ratio of Al and Cr_2O_3 was 2:1, the content of SiC was changed to mix the powders. Four groups of Cr_2O_3-Al-SiC composite powders with different SiC content were prepared by spray drying technology. The proportion of raw materials in the composite powders is shown in Table 1. CAS5, CAS12, CAS19 and CAS30 represented the composite powders with SiC content of 5, 12, 19 and 30 wt.%, respectively.

Table 1 Proportion of raw materials in Cr_2O_3-Al-SiC composite powders

Composite powders (wt.%)	Cr_2O_3	Al	SiC
CAS5	70	25	5
CAS12	65	23	12
CAS19	60	21	19
CAS30	52	18	30

The coatings prepared by the four groups of composite powders were marked as CCAS5, CCAS12, CCAS19 and CCAS30, respectively.

$$Cr_2O_3 + 2Al = Al_2O_3 + 2Cr \quad \text{(Eq 1)}$$

TC4 (Ti6Al4V) titanium alloy (Beijing Qianshuo Nonferrous Metal Products Co., Ltd., China) was selected as the matrix, and the sample size was 10 mm × 10 mm × 12 mm. The substrate was gristblasted to obtain a clean and rough surface before spraying. The GP-80 type plasma spraying system (Jiujiang Spraying Device Co., Ltd., China) was used to prepare the coatings. NiCrAlY powder (Hangtian Zhenbang Technology Co., Ltd.) was sprayed on the surface of the substrate as a bonding layer to reduce the residual stress caused by the TEC mismatch and increase the bonding strength between the coating and the substrate. NiCrAlY powder consists of 72.5 wt.% Ni, 17 wt.% Cr, 10 wt.% Al and 0.5 wt.% Y, with particle size of -200 ~ + 500 mesh. The plasma spraying parameters of the coatings are shown in Table 2.

The phase compositions of the composite powders and coatings were determined by x-ray diffractometer (Rigaku DMAX-2500) with Cu Kα radiation. The working mode of the diffractometer was continuous scanning, the power was 6 kW, the scanning speed was 4°/min and the scanning range was from 20 to 80°. The scanning electron microscope (SEM, Hitachi S-4800) equipped with the EDAX-AMETEK energy spectrometer (EDS) was used to characterize the morphology of the powders and the cross-sections of the coatings. Image analysis method was used to analyze the porosity of the coatings, with 10 cross-sectional scans at 500 × magnification selected on each coating. The hardness of the coating was measured using a microhardness tester (SHIMADZU HMV-2) with Vickers diamond pyramid indenter. The load was 0.1 kgf, and the dwell time was 15 s. In order to reduce the error, the average value of 20 points was selected as the hardness value of the coatings. The toughness of the coatings was analyzed by the indentation method at 0.5 kgf and 2 kgf, and the dwell time was 15 s. Under 2 kgf load, the radial cracks in the indentation corners were well developed and repeatable. Three points of each coating were randomly selected, and the indentation half-diagonal and crack length of each indentation were measured and averaged. The fracture toughness was calculated as follows (Ref 27, 28):

$$K_{IC} = 0.079\frac{P}{a^{3/2}}\log(4.5\frac{a}{c})\ 0.6\ \leq c/a \leq 4.5 \quad \text{(Eq 2)}$$

where P is the applied load (N), a is the indentation half-diagonal and c is the crack length from the center of the indent.

Results and Discussion

Phase and Microstructure Analysis of Composite Powders

Figure 1 shows the XRD pattern of CAS12 composite powders obtained by spray drying. The composite powders were composed of Cr_2O_3, Al and SiC phases. Figure 2 shows the SEM micrographs of CAS12 composite powders and the element composition of the area A in Fig. 2(b). The powders were spherical with smooth surface and dense structure. The particle size was about 30-60 μm and evenly distributed. The composite powders had good surface quality and no obvious defects. These powders had good fluidity, which were conducive to atmospheric plasma spraying (Ref 29). Figure 2(c) shows that the element composition of the powder was Cr, Al, O, C and Si. The constituent elements of the composite powders were the same as the raw powders. Combined with the XRD results in Fig. 1, it can be further determined that the composite powders were composed of Cr_2O_3, Al and SiC.

From the above analysis, it can be seen that the composite powders prepared by spray drying technology had no phase transition. Spray drying ensured good agglomeration and uniform distribution of raw powders, which can avoid the separation of raw powders in the plasma jet. Each agglomerated particle was a substantial SHS reaction unit during spraying, and its agglomerated structure was conducive to the ignition of SHS reaction in RPS process and the adequate conduct of the reaction during spraying, so as to form a composite coating with uniform structure in situ (Ref 20).

Phase Analysis of Composite Coatings

Figure 3 shows the XRD patterns of the coatings prepared by four groups of Cr_2O_3-Al-SiC composite powders. The relative contents of each phase in the four coatings were calculated according to the reference intensity ratio (RIR) of the characteristic peak, and the results are shown in Table 3. The calculation method is as follows:

Table 2 The plasma spraying parameters of the coatings

Parameters	NiCrAlY bond coating	Composite coating
Arc voltage (V)	60	70
Arc current (A)	500	500
Primary gas flow rate (Ar, dm^3 /min)	120	150
Second gas flow rate (H_2, dm^3 /min)	30	30
Powder flow rate (L/min)	0.4	0.4
Spraying distance (mm)	100	100

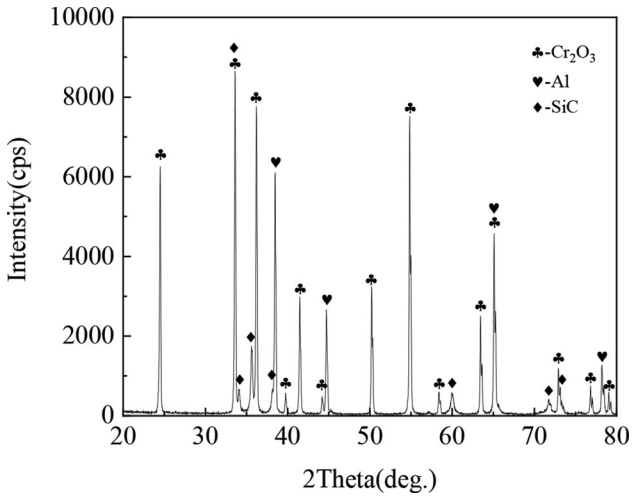

Fig. 1 XRD pattern of CAS12 composite powders

$$W_A = \frac{\frac{I_A}{K_S^A}}{\sum_{i=1}^{n} \frac{I_i}{K_s^i}} \quad \text{(Eq 3)}$$

W_A: relative content of A phase, I_A: integral intensity value of the strongest diffraction peak of A phase and K_S^A : reference intensity ratio (RIR) value of A phase.

It is shown from Fig. 3 that the Cr_7C_3, $CrSi_2$ and Al_2O_3 phases were synthesized in situ in plasma jet. The reaction can be expressed as Eq. 4. However, Cr_3C_2, Cr_3Si and CrSi by-products were also formed in this process, indicating that the reaction of Cr_2O_3-Al-SiC system in the plasma jet was relatively complex (Ref 14). In the Cr-C system, the Gibbs free energy of Cr_3C_2 ($\Delta G_f = -112.9$ kJ/mol) is higher than that of Cr_7C_3 ($\Delta G_f = -209.2$ kJ/mol), and the most stable $Cr_{23}C_6$ ($\Delta G_f = -481.2$ kJ/mol) should be formed by low-temperature aging treatment (Ref 6). Cr_3C_2 and Cr_7C_3 are orthogonal structures with similar mechanical properties. Their uniform distribution in the coating can improve the microhardness of the coating. As we all know, the preparation of coating by plasma spraying is a process of high temperature, high speed and rapid cooling. The reaction between reactant powders in the spraying process is uncontrollable to a certain extent, the reaction products are diverse and it is easy to form metastable and amorphous phases. The obtained coating presents a multiphase heterogeneous metastable lamellar structure. The literature (Ref 21) also had relevant reports on the Al-Cr_2O_3 aluminothermic reaction system. Without the addition of SiC, the plasma sprayed Al-Cr_2O_3 system not only reacted to produce Cr and Al_2O_3, but also generated the continuous solid solution (Al, Cr)$_2O_3$ phase of Al_2O_3 and Cr_2O_3. The (Al, Cr)$_2O_3$ phase was not found in this study, which may be due to the addition of SiC changing the direction of the reaction. The literature (Ref 30) pointed out that the reaction products of thermite reaction system are closely related to the composition of reactants, reaction degree and cooling conditions.

$$17Cr_2O_3 + 34Al + 12SiC = 4Cr_7C_3 + 6CrSi_2 + 17Al_2O_3 \quad \text{(Eq 4)}$$

As shown in Table 3, with the increase of SiC content in the composite powder, the content of SiC in the coating also increased gradually. There were more raw materials Cr_2O_3 and Al in CCAS5 coating, and the desired phases of Cr_7C_3 and Al_2O_3 was less, which indicated that the reaction of CAS5 composite powder in plasma jet was insufficient, so that a large amount of Cr_2O_3 and Al was remained. Since the adiabatic temperature of the reaction between Cr_2O_3 and Al is greater than 1800 K, the reaction can proceed spontaneously. The insufficient reaction may be due to the addition of 5 wt.% SiC inhibited the reaction. As the SiC content in the composite powder increased to 12 wt.%, the content of Cr_2O_3 and Al in the coating decreased, and the content of γ-Al_2O_3 and Cr_7C_3 increased. This was because increasing the amount of SiC allowed SiC to fully react with the aluminothermic reaction product Cr to produce chromium carbide and chromium silicide. The reactions can be expressed as (5), (6) and (7). This process consumed the reaction products of aluminothermic reaction and promoted the forward progress of the reaction. CCAS19 and CCAS30 coatings had a large amount of SiC, indicating that a large amount of SiC was not involved in the reaction. This showed that when the SiC content was 12 wt.%, the reaction was relatively sufficient.

$$17Cr + 6SiC = 2Cr_7C_3 + 3CrSi_2 \quad \text{(Eq 5)}$$

$$32Cr + 6SiC = 2Cr_7C_3 + 6Cr_3Si \quad \text{(Eq 6)}$$

$$10Cr + 3SiC = Cr_7C_3 + 3CrSi \quad \text{(Eq 7)}$$

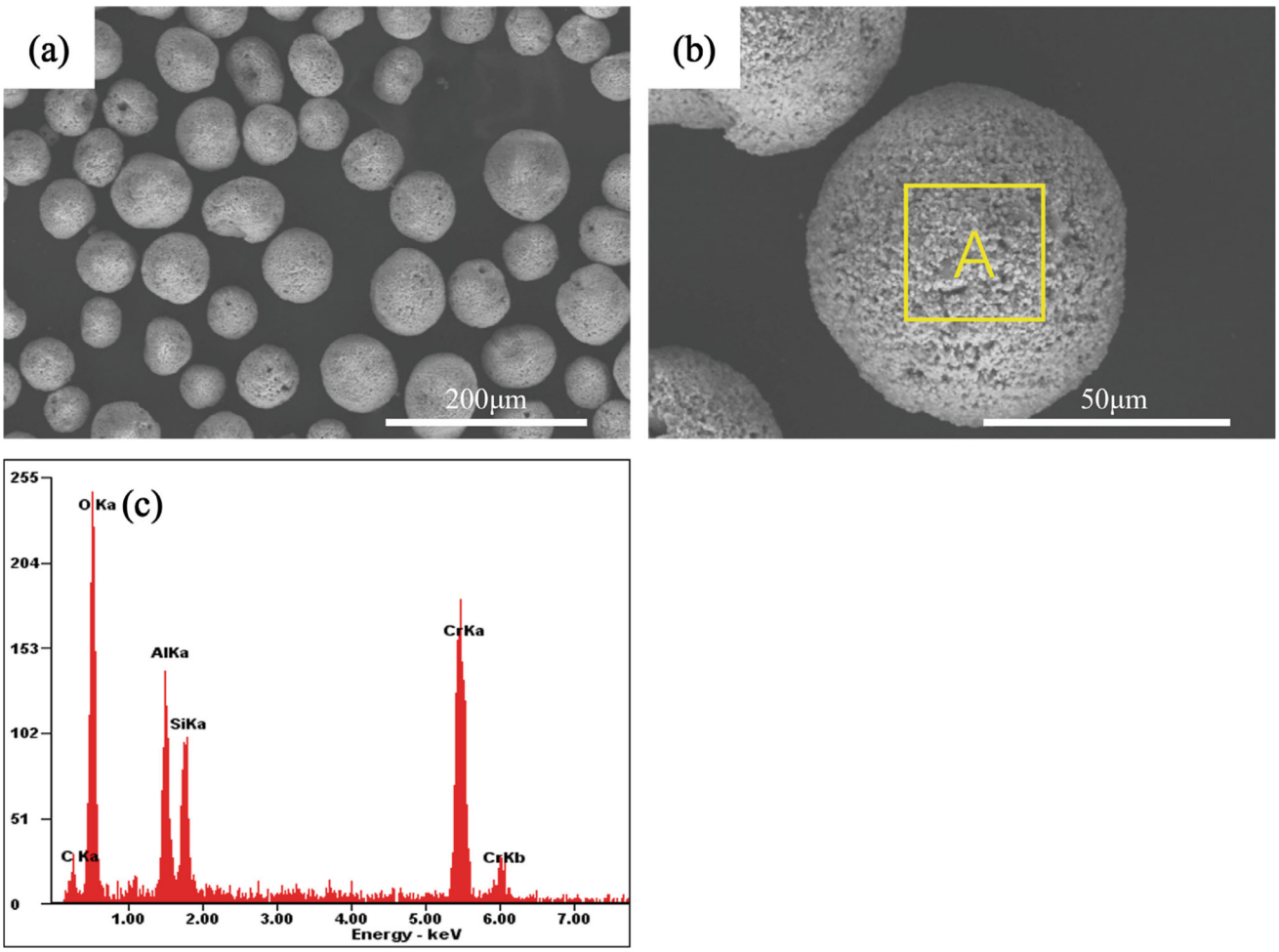

Fig. 2 SEM micrographs and EDS pattern of CAS12 composite powders: (a) SEM of CAS12 composite powders, (b) high magnification of (a) and (c) EDS pattern of area A

Microstructure Analysis of the Chromium Carbide Composite Coatings

Figure 4 shows the cross-sectioned SEM image of the coatings prepared by Cr_2O_3-Al-SiC composite powder with different SiC content. In the process of plasma spraying, the feedstock powders melted in the plasma jet and reactions occurred in the droplets. The reacted droplets crashed onto the surface of substrate at a high speed, followed by rapid spread and solidification on the substrate to form the lamellar and splat-like structure (Ref 25). From Fig. 4(a), (c), (e) and (g), it can be seen that the as-prepared four coating samples showed obvious three layers. The upper layer was ceramic coating, the middle layer was bonding layer and the bottom layer was TC4 titanium alloy substrate. As shown in Fig. 4(b), (d), (f) and (h), the wave lamellar structure of the coatings becomes less and less obvious with the increase of SiC content. In particular, CCAS30 coating (see Fig. 4(h)) had large holes and cracks, and almost no lamellar structure can be observed. The microstructure of the four coatings was mainly composed of black, dark gray and light gray areas. Table 4 shows the EDS results for the three areas shown in Fig. 4(d). Black area A was mainly rich in Al and O, light gray area B was mainly rich in Cr, C and O and dark gray area C was rich in Cr and Si. Combined with the XRD results of the coating, it can be known that the A region was mainly composed of Al_2O_3 and Al, B area was mainly composed of Cr_7C_3, Cr_3C_2 and Cr_2O_3 and C area was mainly composed of various Cr-Si compounds.

It is shown from Fig. 4(b) that CCAS5 coating was relatively dense, with obvious lamellar structure. According to the XRD in Fig. 3(a) and the phase content calculation results in Table 2, it was known that a large amount of Al (10.6 wt.%) remained in the coating. The melting point of Al was low, which provided a good liquid environment in the plasma jet and promoted the spread of the droplets. However, some pores formed by volume

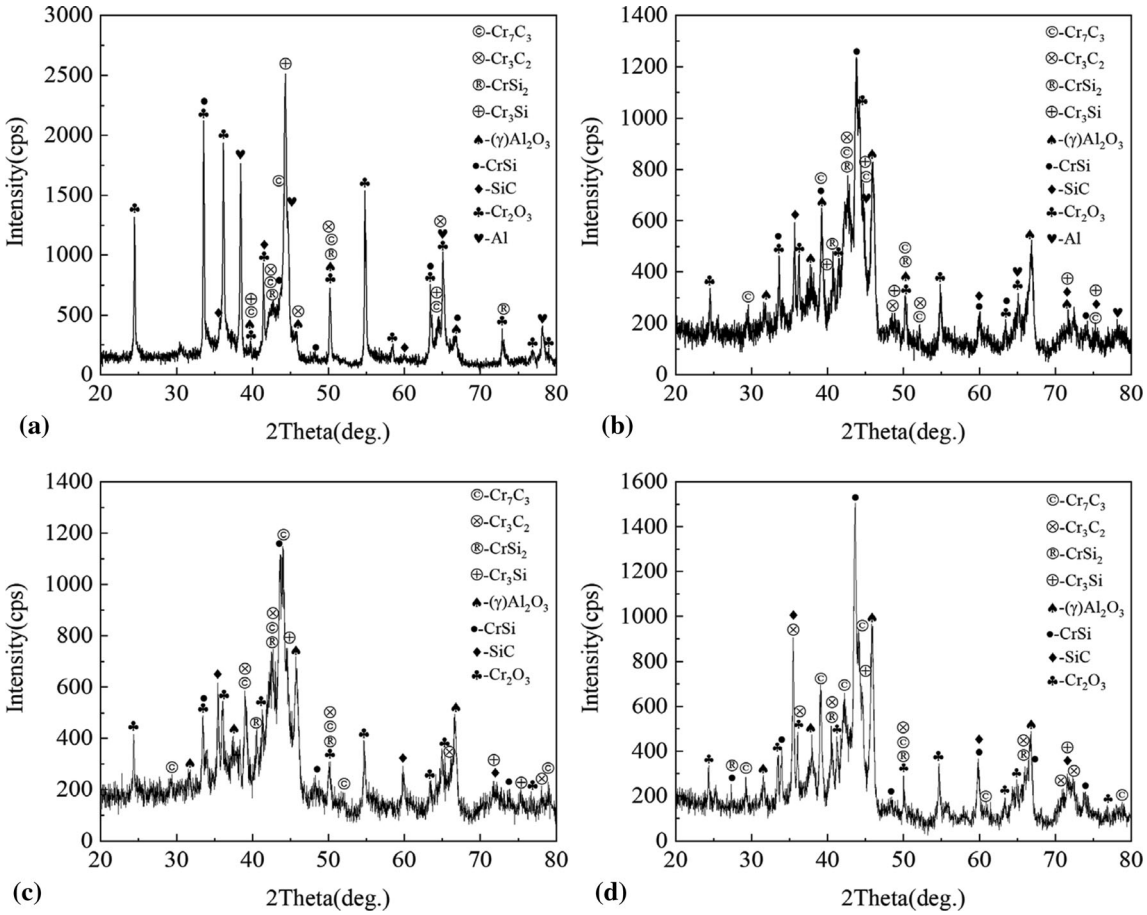

Fig. 3 XRD patterns of four coatings: (a) CCAS5, (b) CCAS12, (c) CCAS19 and (d) CCAS30

Table 3 Phase content calculation results of four coatings

Coatings	Phases, wt.%								
	Cr_2O_3	Al	SiC	Cr_7C_3	Cr_3C_2	γ-Al_2O_3	$CrSi_2$	Cr_3Si	CrSi
CCAS5	28.7	10.6	2.1	16.6	8.0	12.8	4.4	6.6	10.2
CCAS12	7.8	4.3	3.8	31.0	10.5	27.5	5.1	3.3	6.7
CCAS19	6.4	…	8.9	29.2	10.8	27.9	6.1	3.7	7.0
CCAS30	6.2	…	14.7	26.9	10.3	26.3	4.6	2.9	8.1

shrinkage during solidification of droplets can also be observed. With the SiC content in the composite powder increasing, it can be seen that the structure of CCAS12 coating was evenly distributed and dense. The coating had obvious lamellar structure, and there were almost no holes in the coating, and the overall quality of the coating was good. When the SiC content in the composite powder increased to 19 wt.%, Al disappeared and the SiC content in the coating increased. From Fig. 4(e) and (f), it can be seen that the lamellar structure of the coating became thicker, the number of pores increased significantly and the coating quality decreased. After further increasing the content of SiC in the composite powder, the compactness of CCAS30 coating was very poor, there were many unmelted particles in the coating and the lamellar structure was not obvious. According to the phase content calculation results in Table 2, there was a large amount of SiC (14.7 wt.%) remained in the coating. Yeh et al. (Ref 31) carried out SHS experiment on compressed samples prepared from Cr_2O_3-2Al-ySi (y = 0.67-4.0) powder mixtures. The results showed that with the increase of Si content, the combustion wave velocity decreased, and the adiabatic temperature of the system decreased from 1960 to 1575 K. This showed that with the increase of Si content, the heat released by aluminothermic reaction will decrease. Through calculation, it can be seen that the adiabatic temperature of Cr and SiC reaction is less than 1800 K, the reaction cannot be self-sustaining and the external energy

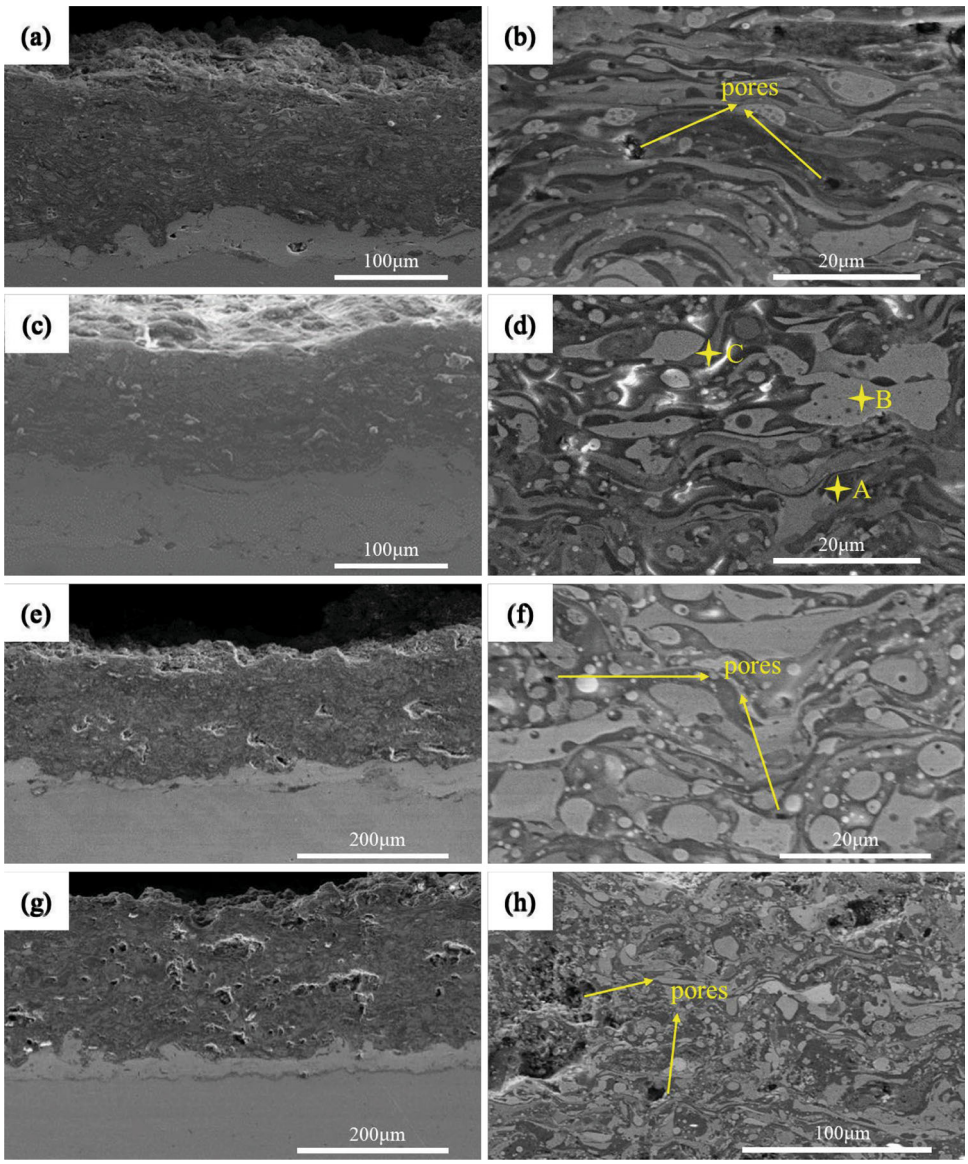

Fig. 4 Cross-sectional micrographs of four coatings: (a) CCAS5, (c) CCAS12, (e) CCAS19, (g) CCAS30, (b), (d), (f) and (h) high magnification of (a), (c), (e) and (g)

Table 4 EDS results of the area shown in Fig. 4(d)

Elements(wt.%)	Cr	Si	C	Al	O
A	8.80	0.72	4.70	47.93	37.86
B	73.04	1.54	12.00	1.03	12.39
C	42.76	36.13	9.40	4.07	7.64

must be continuously provided for the reaction (Ref 14). In this study, the excess SiC in the CAS30 raw material powder led to the reduction of the heat released by the aluminothermic reaction. On the one hand, it was not conducive to the reaction between Cr and SiC, and on the other hand, the melting point of SiC (2700 °C) is high, and the presence of a large amount of SiC led to insufficient melting of the powder system. When the droplets with unmelted particles crashed the substrate, they were not fully spread. The accumulation of a large number of unmelted particles led to high porosity of the coating. The coating showed the characteristics of loose microstructure and poor quality.

Figure 5 shows the porosity of the four coatings. The porosity of the coating is an important indicator of the quality of the coating. The formation of pores in APS coating is mainly due to the following reasons (Ref 32, 33): One is the gas in the droplets did not escape from the deposits, the second is the volume shrinkage of droplets during solidification and the third is the incomplete overlap of droplets when they crashed the substrate. With the increase of SiC content, the porosity of the composite coatings decreased first and then increased. The porosity of

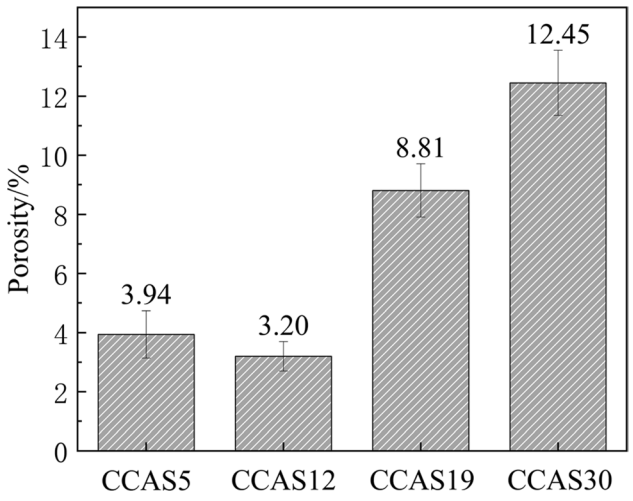

Fig. 5 Porosity of four coatings

CCAS12 coating was the lowest, only 3.20%, and the porosity of CCAS30 coating was the highest, which was 12.45%. When the SiC content was low (5 wt.%), there was more Al remained in the coating. The volume shrinkage caused by solidification of a large amount of molten Al was so serious that the porosity of the coating was high. When the SiC content was high (19 and 30 wt.%), there was more unreacted SiC in the coating. The existence of unmelted particles made the droplets spread inadequately, resulting in high porosity. The quality of APS coating has a great relationship with the melting state of feedstocks and the characteristics of molten raw material particles (Ref 34). With the increase of SiC content in the composite powder, the reaction degree and melting state of the feedstocks will change during the plasma spraying process, resulting in the coating quality increased first and then decreased. It can be concluded that the composition of composite powder plays an important role in regulating and controlling the structure of the coating.

Formation Mechanism of the Chromium Carbide Composite Coatings

Combining the characteristics of the reactant powders, the XRD results of the coatings and the cross-sectional SEM of the coatings, the qualitative mechanism of the reaction of Cr_2O_3-Al-SiC composite powder in the plasma jet during plasma spraying can be proposed, as shown in Fig. 6. After the feedstock particles enter the plasma jet, the Al with low melting point first melts. Molten Al wraps unmelted Cr_2O_3 and SiC, providing a good liquid-phase environment for the reaction system and making full contact between components. The preferential formation of molten phase not only enhances the interaction between reactants, but also leads to the densification of the final coating. Then, Al reacts with unmelted Cr_2O_3 (2435 °C) to form Cr and Al_2O_3. The heat released by the reaction and the heat of plasma jet are superimposed to promote the melting of powder particles and accelerate the reaction. Then, Cr reacts with SiC to produce chromium carbide and chromium silicide. Finally, driven by the plasma flow, the molten droplets quickly crash the substrate, resulting in deformation, diffusion and finally cooling and solidification. Multiple droplets accumulate continuously on the surface of the substrate and finally form a coating. The reaction process of the four groups of composite powders in the plasma jet is the same, and they all experienced four processes: melting, diffusion, reaction and deposition. However, due to the different content of SiC in the composite powder, the microstructure of the coating obtained is different.

Performance Characterization of the Chromium Carbide Composite Coatings

Microhardness Analysis of the Chromium Carbide Composite Coatings

The microhardness of coating is mainly affected by two factors: One is the phase of the coating, and the other is the microstructure of the coating. Generally, the increase of the content of hard phases in the coating contributes to the increase of microhardness, and the increase of the coating density contributes to the increase of microhardness (Ref 35). The average microhardness of CCAS5, CCAS12, CCAS19 and CCAS30 coatings was 821.1 $HV_{0.1}$, 1262.2 $HV_{0.1}$, 1029.6 $HV_{0.1}$ and 820.4 $HV_{0.1}$, respectively. It can be found that with the increase of SiC content, the average microhardness of the coatings first increased and then decreased. The CCAS12 coating had the highest microhardness. Because the ceramic coating prepared by plasma spraying is a kind of heterogeneous material, the indentation will encounter different microstructure at different positions. The microhardness value will vary with the indentation position. Therefore, the average value of microhardness cannot really reflect the characteristics of hardness. Using Weibull distribution can more accurately describe the microhardness distribution of coating. The Weibull distribution of the microhardness values of the four coatings and their corresponding fitted straight lines are shown in Fig. 7. The higher the slope of the fitted straight line, the more uniform the microstructure distribution of the coating and the more stable the performance of the coating. With the increase of SiC content, the slope of the fitted straight lines first increased and then decreased. The slope of CCAS12 coating (9.5) was the highest, indicating that the microhardness distribution of CCAS12 coating was more uniform, and the coating quality was more homogeneous.

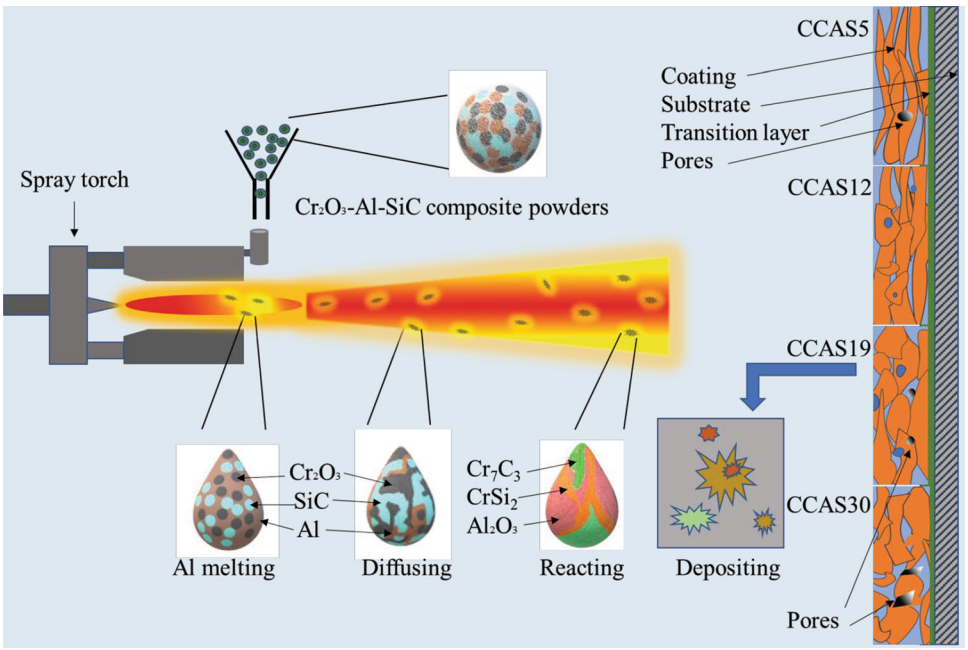

Fig. 6 Formation mechanism diagram of the coatings prepared by plasma spraying Cr_2O_3-Al-SiC composite powders

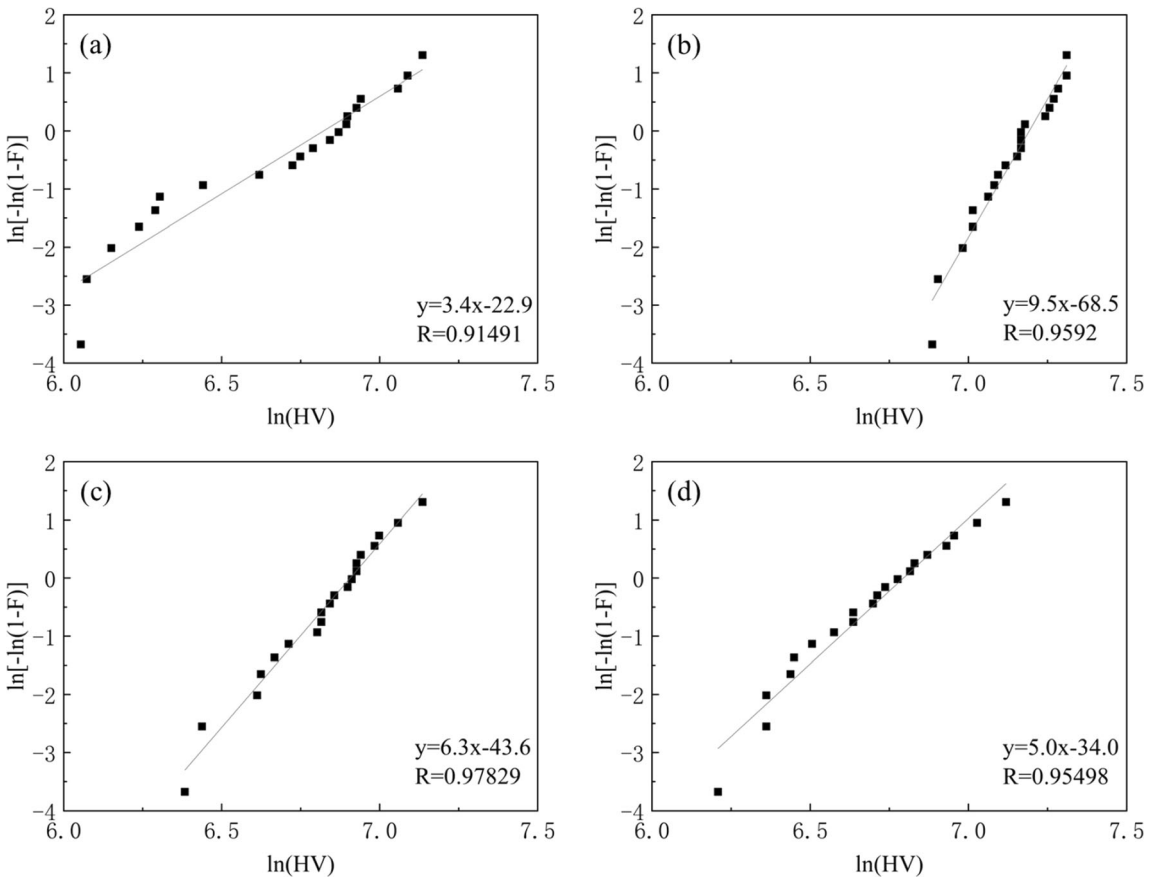

Fig. 7 Weibull distribution of the microhardness values and corresponding fitting straight lines of four coatings: (a) CCAS5, (b) CCAS12, (c) CCAS19 and (d) CCAS30

When the SiC content was 5 wt.%, the reaction degree of CAS5 composite powder was low, and a large amount of Al remained in the coating. Although the total content of hard phase Cr_7C_3 and Cr_3C_2 in the coating reached 24.6

wt.%, a large amount of Al diluted the overall hardness of the coating. When the SiC content was too high (19 and 30 wt.%), there was a large amount of unmelted SiC in the coating. The microstructure of the coating was loose and the porosity was high. The non-uniformity of phase distribution and the existence of defects in the coating made the microhardness of the coating discrete, so the average microhardness of the coating decreased. When the SiC content was 12 wt.%, the coating structure was uniform and dense, and the hard phase was evenly distributed, so it had high microhardness.

Toughness Analysis of the Chromium Carbide Composite Coatings

The indentation fracture examination of the coatings was carried out with a load of 0.5 kgf and a load of 2 kgf. Figure 8 shows the indentation morphology of four coatings under 0.5 kgf load. Under the same magnification, the indentation area of CCAS12 coating was obviously the smallest, which is consistent with the results of microhardness. As shown in the figure, the indentation of the four coatings was relatively intact, without large radial cracks. However, some small cracks can be seen on the edges of the indentation of CCAS5, CCAS19 and CCAS30 coatings, and the edges of the indentation of CCAS30 coating were warped. No obvious cracks were observed around the indentation of CCAS12 coating. This shows that the CCAS12 coating had better toughness.

Figure 9 shows the crack morphology at the indentation corner of the coatings under 2 kgf load. After increasing the load, obvious cracks appeared on the indentation edge (marked by blue arrows) and corner (marked by yellow oval) of the four coatings. There was obvious collapse and warping around the indentation of CCAS19 and CCAS30 coatings. The fracture toughness of CCAS5, CCAS12, CCAS19 and CCAS30 coatings was calculated to be 2.8, 3.3, 2.5 and 1.7 MPa $m^{1/2}$, respectively. CCAS5 and CCAS12 coatings had higher fracture toughness than CCAS19 and CCAS30 coatings, and CCAS12 coating had the best fracture toughness.

There are two reasons for the poor toughness of CCAS19 and CCAS30 coatings. One is that there are a large number of unmelted or semi-melted particles in the coating, resulting in poor compactness of the coating. The other is that there is a large amount of unreacted SiC in the coating. SiC ceramics have obvious brittleness. The presence of large amounts of SiC in the coating reduces toughness of the coating (Ref 36, 37). Due to complete reaction and full melting of composite powder, CCAS12 coating had homogeneous and dense structure. Uniform and dense coating structure contributes to reduce stress concentration and improve crack propagation force (Ref 19). Therefore, CCAS12 coating had high toughness.

Conclusions

Four groups of Cr_2O_3-Al-SiC composite powders with different SiC content (5, 12, 19 and 30 wt.%) were prepared by spray drying technology; then, four kinds of chromium carbide composite coatings were successfully

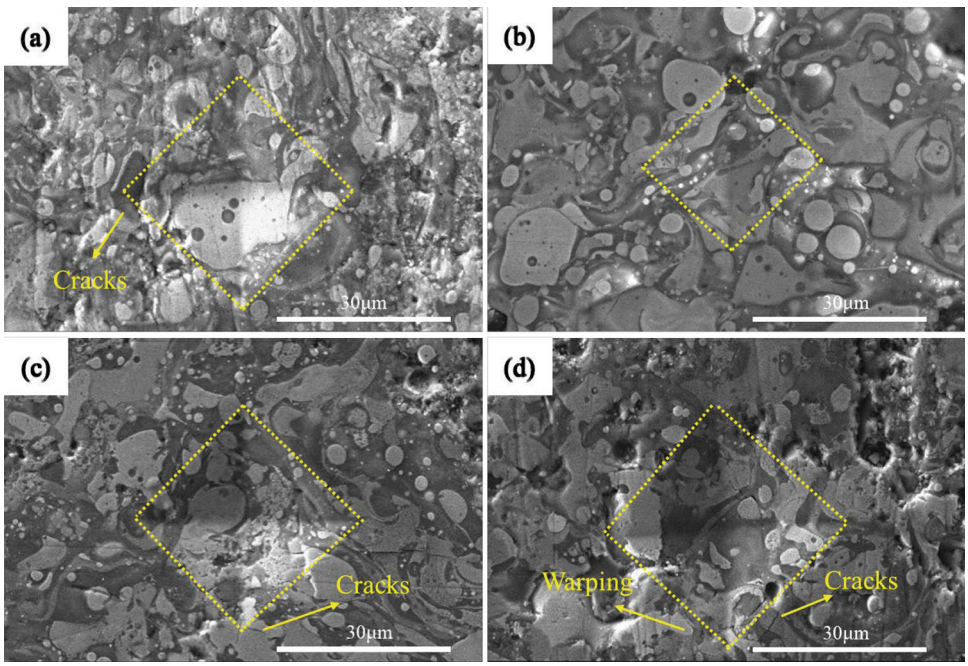

Fig. 8 Indentation micrographs of four coatings (load 0.5 kgf): (a) CCAS5, (b) CCAS12, (c) CCAS19 and (d) CCAS30

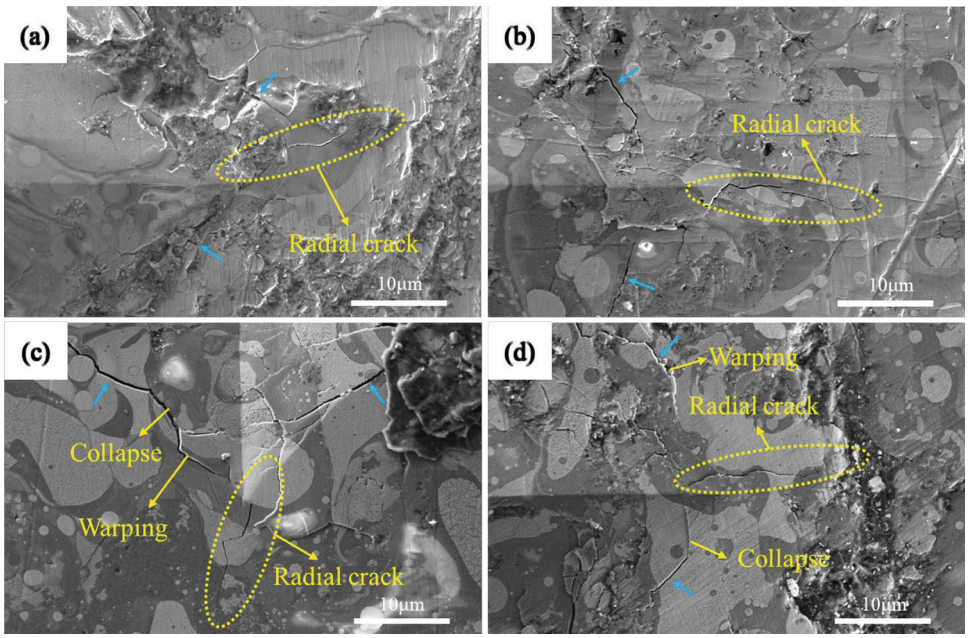

Fig. 9 Crack morphology at indentation corner of four coatings (load 2 kgf): (a) CCAS5, (b) CCAS12, (c) CCAS19 and (d) CCAS30

prepared on the surface of TC4 titanium alloy by plasma spraying. The effects of SiC content on the microstructure and properties of the coatings were investigated. The conclusions are as follows:

(1) The four groups of composite powders obtained by spray drying had obvious reactions in the plasma jet, and the desired phases of Cr_7C_3, $CrSi_2$ and Al_2O_3 were produced in the coatings with some by-products. When the SiC content was 5 wt.%, the reaction of the raw powders in the plasma jet was not sufficient, and a large amount of raw powders Cr_2O_3 and Al was remained in the coating. When the SiC content was 12 wt.%, the reaction was relatively sufficient, and the residual raw powders were less. When the SiC content was 30 wt.%, there was a large amount of unreacted SiC in the coating.

(2) With the increase of SiC content, the porosity of the coatings decreased first and then increased. When the SiC content was 12 wt.%, the microstructure of coating was uniform and dense, and the coating had the lowest porosity of 3.20%.

(3) With the increase of SiC content, the microhardness and toughness of the coatings first increased and then decreased. When SiC content was 12 wt.%, the coating had the highest microhardness (1262.2 $HV_{0.1}$) and the best fracture toughness (3.3 MPa $m^{1/2}$). This was attributed to the high content of hard phase, low porosity and uniform and dense structure of the coating.

Acknowledgments The authors gratefully acknowledge the financial supports of the National Natural Science Foundation of China (52072110) and the Natural Science Foundation of Hebei Province (E2018202034).

References

1. M. Cekada, M. Macek, D.K. Merl and P. Panjan, Properties of Cr(C, N) Hard Coatings Deposited in Ar-C_2H_2-N_2 Plasma, *Thin Solid Films*, 2003, **433**(1-2), p 174-179.
2. M.Y. Niu, Q.L. Bi, J. Yang and W.M. Liu, Tribological Performances of Ni_3Si–Cr_7C_3 Composite Coatings Under Water and Acid Environments, *Tribol. Int.*, 2012, **48**, p 216-225.
3. V. Singh, R. Diaz, K. Balani, A. Agarwal and S. Seal, Chromium carbide–CNT Nanocomposites with Enhanced Mechanical Properties, *Acta Mater.*, 2009, **57**(2), p 335-344.
4. Y.V. Stulov and S.A. Kuznetsov, Synthesis of Chromium Carbide Coatings on Carbon Steels in Molten Salts and their Properties, *Glass Phys. Chem.*, 2014, **40**(3), p 324-328.
5. X.B. Liu and Y.J. Gu, Plasma Jet Clad γ/Cr_7C_3 Composite Coating on Steel, *Mater. Lett.*, 2006, **60**(5), p 577-580.
6. M.Y. Niu, Q.L. Bi, L.Q. Kong, J. Yang, and W.M. Liu, A Study of Ni_3Si-Based Composite Coating Fabricated by Self-Propagating High-Temperature Synthesis Casting Route, *Surf. Coat. Technol.*, 2011, **205**(17-18), p 4249-4253.
7. H.B. Zhu, J. Shen, F. Gao, Y. Yu, and C. Li, Microstructure and Sliding WEAR PERFORMANCE of Cr_7C_3-(Ni, Cr_3(Al, Cr) Coating Deposited from $_Cr_7C3$ In Situ Formed Atomized Powder, *J. Therm. Spray Technol.*, 2016, **26**(1-2), p 254-264.
8. M. Masanta, P. Ganesh, R. Kaul, and A.R. Choudhury, Microstructure and Mechanical Properties of TiB_2–TiC–Al_2O_3–SiC Composite Coatings Developed by Combined SHS, Sol–Gel and Laser Technology, *Surf. Coat. Technol.*, 2010, **204**(21-22), p 3471-3480.
9. M. Masanta, S.M. Shariff, and A.R. Choudhury, Tribological Behavior of TiB_2–TiC–Al_2O_3 Composite Coating Synthesized by Combined SHS and Laser Technology, *Surf. Coat. Technol.*, 2010, **204**(16-17), p 2527-2538.

10. Y.M. Zou, Z.G. Qiu, C.J. Huang, D.C. Zeng, R. Lupoi, N.N. Zhang, and S. Yin, Microstructure and Tribological Properties of Al_2O_3 Reinforced FeCoNiCrMn High Entropy Alloy Composite Coatings by Cold Spray, *Surf. Coat. Technol.*, 2022, **434**, 128205.
11. P.P. Wang, Y.H. Bai, X. Zhao, X.R. Ren, and W.C. Sun, Oxidation Protection of $CrSi_2$-HfB_2-SiC/SiC Coating for Graphite in Variable-Temperature Environment, *Corros. Sci.*, 2022, **199**, 110165.
12. F. Liu, H.J. Li, S.Y. Gu, X.Y. Yao, and Q.G. Fu, Microstructure and Oxidation Property of $CrSi_2$-$ZrSi_2$-Y_2O_3/SiC Coating Prepared on C/C Composites by Supersonic Atmosphere Plasma Spraying, *Surf. Coat. Technol.*, 2019, **374**, p 966–974.
13. A. Moll, S. Laborde, F. Barou, and M. Beaudhuin, Centimetric $CrSi_2$ Crystal Grown by the Vertical Gradient Freeze Method, *J. Cryst. Growth*, 2020, **534**, p 125505.
14. Y.D. Ma, M.Y. Guo, W. Li, Y. Yang, P.Y. Gao, Y.H. Cui, W.W. Sun, Y.W. Wang, L. Wang, and Y.C. Dong, Microstructure and Properties of Cr_7C_3-$CrSi_2$ Composite Coatings Prepared by Plasma Spraying, *Surf. Coat. Technol.*, 2021, **412**, p 127011.
15. V. Carnicer, M.J. Orts, R. Moreno, and E. Sanchez, Microstructure Assessment of Suspension Plasma Spraying Coatings from Multicomponent Submicronic Y-TZP/Al_2O_3/SiC Particles, *Ceram. Int.*, 2018, **44**(11), p 12014-12020.
16. X. Qiao, Y.M. Wang, W.X. Weng, B.L. Liu, and Q. Li, Influence of Pores on Mechanical Properties of Plasma Sprayed Coatings: Case Study of YSZ Thermal Barrier Coatings, *Ceram. Int.*, 2018, **44**(17), p 21564-21577.
17. Y.G. Han, Y. Yang, L. Wang, X.G. Chen, Z.H. Chu, X.N. Zhang, Y.C. Dong, Z. Liu, D.R. Yan, J.X. Zhang and C.G. Li, Microstructure and Properties of in-Situ TiB_2 Matrix Composite Coatings Prepared by Plasma Spraying, *Appl. Surf. Sci.*, 2018, **434**, p 48-54.
18. Y. Yang, D.R. Yan, Y.C. Dong, L. Wang, X.G. Chen, J.X. Zhang, J.N. He, and X.Z. Li, In Situ Nanostructured Ceramic Matrix Composite Coating Prepared by Reactive Plasma Spraying Micro-Sized Al–Fe_2O_3 Composite Powders, *J. Alloys Compd.*, 2011, **509**(5), p L90-L94.
19. L. Wang, D.R. Yan, Y. Yang, Y.C. Dong, X.G. Chen, and J.X. Zhang, Structure and Properties of Nanostructured Ceramic Matrix Composite Coatings Prepared in-Situ by Reactive Plasma Spraying Micro-Sized Al–Fe_2O_3–Cr_2O_3 Powders, *Ceram. Int.*, 2014, **40**(5), p 6481-6486.
20. X.G. Chen, Y. Yang, D.R. Yan, Y.C. Dong, L. Wang, J.N. He, J.X. Zhang, and X.Z. Li, Microstructure and Properties of in Situ Nanostructured Ceramic Matrix Composite Coating Prepared by Plasma Spraying, *J. Mater. Sci.*, 2011, **46**(23), p 7369-7376.
21. D.R. Yan, Y. Yang, Z.H. Chu, X.G. Chen, X.R. Dai, Y.H. Wang, and Y.C. Dong, In Situ Composite Coatings Prepared by Complex Reactive Plasma Spraying of Fe_2O_3-Al-Cr_2O_3 Composite Powders, *Surf. Coat. Technol.*, 2017, **328**, p 94-101.
22. X.L. Wang, Y. Yang, S.T. Jia, Y.W. Wang, Y.D. Ma, Y.H. Cui, X.Y. Wang, W.W. Sun, and L. Wang, In-Situ Synthesis, Microstructure, and Properties of NbB_2-NbC-Al_2O_3 Composite Coatings by Plasma Spraying, *J. Adv. Ceram.*, 2022, **11**(8), p 1263-1278.
23. I. Ozdemir, I. Hamanaka, M. Hirose, Y. Tsunekawa, and M. Okumiya, In Situ Formation of Al-Si-Mg Based Composite Coating by Different Reactive Thermal Spray Processes, *Surf. Coat. Technol.*, 2005, **200**(1-4), p 1155-1161.
24. C. Tekmen, Y. Tsunekawa, and M. Okumiya, Effect of Plasma Spray Parameters on in-Flight Particle Characteristics and in-Situ Alumina Formation, *Surf. Coat. Technol.*, 2008, **203**(3-4), p 223-228.
25. J.Y. Xu, B.L. Zou, X.Z. Fan, S.M. Zhao, Y. Hui, Y. Wang, X. Zhou, X.L. Cai, S.Y. Tao, H.M. Ma, and X.Q. Cao, Reactive Plasma Spraying Synthesis and Characterization of TiB_2–TiC–Al_2O_3/Al Composite Coatings on a Magnesium Alloy, *J. Alloys Compd.*, 2014, **596**, p 10-18.
26. W. Zheng, J.M. Wu, S. Chen, C.S. Wang, C.L. Liu, S.B. Hua, K.B. Yu, J. Zhang, J.X. Zhang, and Y.S. Shi, Influence of Al_2O_3 Content on Mechanical Properties of Silica-Based Ceramic Cores Prepared by Stereolithography, *J. Adv. Ceram.*, 2021, **10**(6), p 1381-1388.
27. A.G. Evans and T.R. Wilshaw, Quasi-Static Solid Particle Damage in Brittle Solids–I Observations Analysis and Implications, *Acta Metall.*, 1976, **24**(10), p 939-956.
28. Y. Liu, T.E. Fischer, and A. Dent, Comparison of HVOF and Plasma-Sprayed Alumina/Titania Coatings–Microstructure, Mechanical Properties and Abrasion Behavior, *Surf. Coat. Technol.*, 2003, **167**(1), p 68–76.
29. Y.Q. Jiang, Q.M. Gong, Z.P. Cai, Y. Shao, D.M. Zhuang, and J. Liang, Fabrication of $CrSi_2$/$MoSi_2$/SiC–Mo_2C Gradient Composite Coating on Mo Substrate and the Stabilizing Effect of Cr on the Coating's Anti-Oxidation Properties, *Surf. Coat. Technol.*, 2015, **282**, p 188-199.
30. L. Duraes, B.F.O. Costa, R. Santos, A. Correia, J. Campos, and A. Portugal, Fe_2O_3/Aluminum Thermite Reaction Intermediate and Final Products Characterization, *J. Mater. Sci. Eng. A.*, 2007, **465**(1-2), p 199-210.
31. C.L. Yeh and J.Z. Lin, Combustion Synthesis of Cr–Al and Cr–Si Intermetallics with Al_2O_3 Additions from Cr_2O_3–Al and Cr_2O_3–Al–Si Reaction Systems, *Intermetallics*, 2013, **33**, p 126-133.
32. R. Venkataraman, G. Das, S.R. Singh, L.C. Pathak, R.N. Ghosh, B. Venkataraman, and R. Krishnamurthy, Study on Influence of Porosity, Pore Size, Spatial and Topological Distribution of Pores on Microhardness Of as plasma sprayed ceramic coatings, *Mater. Sci. Eng. A.*, 2007, **445**, p 269-274.
33. D. Thirumalaikumarasamy, V. Balasubramanian, and S.S. Sabari, Prediction and Optimization of Process Variables to Maximize the Young's Modulus of Plasma Sprayed Alumina Coatings on AZ31B Magnesium Alloy, *J. Magnesium Alloys.*, 2017, **5**(1), p 133-145.
34. S. Guessasma and C. Coddet, Microstructure of APS Alumina–Titania Coatings Analysed using Artificial Neural Network, *Acta Mater.*, 2004, **52**(17), p 5157-5164.
35. N. Krishnamurthy, M.S. Murali, B. Venkataraman, and P.G. Mukunda, Characterization and Solid Particle Erosion Behavior of Plasma Sprayed Alumina and Calcia-Stabilized Zirconia Coatings on Al-6061 Substrate, *Wear*, 2012, **274**, p 15-27.
36. T. Schlech, S. Horn, C. Wijayawardhana, and A. Rashidi, Experimental and FEM Based Investigation of the influence of the Deposition Temperature on the Mechanical Properties of SiC Coatings, *J. Adv. Ceram.*, 2021, **10**(1), p 139-151.
37. Z.F. Zhang, J.J. Sha, Y.F. Zu, J.X. Dai, and Y.J. Liu, Fabrication and Mechanical Properties of Self-Toughening ZrB_2–SiC Composites from in-Situ Reaction, *J. Adv. Ceram.*, 2019, **8**(4), p 527-536.